Quantifying Aggregation of Emitter Molecules in Organic Light Emitting Diodes Using Spatial Statistics

Department of Physics, Colorado School of Mines

Galen Vincent

Advisor: Dr. Jeramy Zimmerman

April 25$^{\text{th}}$, 2019

1 Introduction

The electronics industry uses organic light emitting diodes (OLEDs) to create displays that outperform traditional light sources like inorganic LEDs and liquid crystal displays (LCDs) in both efficiency and lifetime [1]. An active area of research within the OLED community is quantifying the molecular structure of devices in order to increase this efficiency and lifetime further. Molecular structure is known to impact performance of OLEDs, but the exact mechanisms are still largely unknown. Figuring out these relationships between structure and performance will allow for the design of better OLEDs. One structure that is thought to negatively impact performance is the aggregation of a specific type of molecules within the emissive layer into clusters [2]. One way to quantify this clustering behavior is to use atom probe tomography (APT), which is a material measurement method that simultaneously measures 3D spatial molecule positions and chemical identity [3].

Aggregation of molecules in APT data is not always immediately evident. To find more subtle clustering patterns, spatial statistics can be used to analyze the trends in molecule position relationships. Other computer algorithms allow for the isolation and study of individual clusters in the data [4, 5, 6]. Applying APT to organic materials hasn't been largely explored yet, so 3D spatial data for OLEDs has not been available, and these methods have never been used to study aggregation within OLED devices.

In this paper, we explore how spatial statistics can be applied to OLED APT data in order to quantify aggregation within the OLED materials. Specifically, we explore the K-function as a possible technique for extracting aggregation properties such as cluster size, shape, density, and spacing by applying it to simulated clustered data. The results from this research can be used to inform the design of more energy efficient and longer lasting OLEDs.

2 Background

2.1 Organic Light Emitting Diodes

OLEDs are semiconductor devices that are fabricated by depositing films of different materials into a device stack. The most crucial of these layers are the anode, cathode, and emissive layers. The emissive layer is made of organic molecules, a small percent of which are responsible for light generation. These are called the emitter molecules, and the rest are called host molecules. There are other layers sometimes used in OLED stacks to increase efficiency, including the injection and transport layers. [1]

To generate light, a voltage is applied across the anode and cathode of the OLED. When this happens, electrons and holes are sent into the emissive layer. A hole is a term used to describe the lack of an electron in a molecular orbital, and can be thought of like an empty pocket waiting to be filled with an electron. Electrons and holes pair up on emitter molecules to form excitons, which are coulombically bound pairs of one electron and one hole. In excitons, the electrons live in the highest occupied molecular orbital (HOMO) of the emitter molecule, and the holes live in the lowest unoccupied molecular orbital (LUMO). When an exciton recombines, the electron drops into its associated hole, and the energy difference between the HOMO and the LUMO is released, often as a photon in the visible

spectrum with wavelength (i.e. color) corresponding to its energy [7]. Emitter molecules are chosen with specific properties so that a very high percent of the exciton recombinations result in photon emission.

The quantum state of the electron in an exciton impacts the mechanism by which it decays [2, 7]. If two emitter molecules are too close together within the emissive layer, triplet-triplet annihilation (TTA) may occur [2]. This is when two electrons in triplet states are close enough to one another that one transfers its energy directly to the other. If this happens, the first electron falls to the LUMO without emitting light, and the second rises to an energy level higher than the HOMO. As the first electron drops to the LUMO without emitting light, TTA can have at most 50% efficiency for light emission. The high energy electron can break bonds in the emitter molecule and damage it permanently, leading to device degradation [8]. When the high energy electron relaxes to the LUMO, it may emit light [2, 7]. Aggregation of the emitter molecules brings them closer to one another, which brings the electrons closer to one another, which leads to more TTA. As a result of this, aggregation leads to lower efficiency and more degradation of the OLED. Due to this structure-performance relationship, quantifying clustering of emitter molecules in the emissive layer is of interest to the OLED research community.

2.2 Atom Probe Tomography

APT is a method that is used to gather high resolution spatial and chemical data from a material sample. The measurement process begins by placing the material sample, a few ten nanometers thick, on a metal tip. This tip is then placed in a vacuum chamber, oriented so the material faces a high resolution position sensitive ion detector. A DC voltage is then applied to the tip. This voltage produces a large electric field in the region between the tip and the detector. The magnitude of this electric field is chosen so that it is just below the evaporation field for the material being studied. The evaporation field is the magnitude of electric field at which the molecular ions begin to "evaporate" off of the bulk material due to the forces from the field. [3]

Once the voltage has been turned on, the sample is pulsed with small spikes of energy so that one ion per pulse has the energy to eject from the material. This is done with either a voltage pulse or a laser pulse. Each ion leaves the material, accelerated by the electric field, and strikes the detector. This detector records the position where the ion lands and the time of flight (TOF) of the ion from when it left the material. Using the hit position and a model of the electric field, the original 3D position of the ion within the material sample is calculated. Using the TOF, the charge to mass ratio of the ion is calculated, which can then be used to identify chemical composition. In the end, a 3D point cloud of molecule positions and identity is obtained. [3] APT can have up to 80% measurement efficiency [9], meaning that 80% of the molecules from the original sample will be present in the reconstruction.

APT has not been used to study organic molecules extensively due to the fact that many organic materials are polymer based. The chain structure of polymers in a material makes it so samples fragment during evaporation [9], leading to poor APT data. However, application of APT to small molecule non-polymer organic materials has recently been shown by our group to produce successful chemical identification and spatial data to a resolution of $\sim$0.3nm in z and $\sim$1nm in x and y [9]. The coordinate system is defined so that the

xy-plane lies parallel to the detector. This resolution is around the size of the particles in OLED devices, which means that APT has the potential to be used for informative analysis regarding structure and aggregation behavior in OLEDs.

2.3 Cluster Detection and Characterization Methods

The data collected from APT can be analyzed to identify and quantify aggregation within materials. One method of doing so is using spatial statistics, which is used to analyze the general relationships between points in a data set. One function that is particularly useful for detecting clustering behavior in spatial data is Ripley's K-function. This function calculates the average number of points that lie within a certain radius of any original point, normalized by the density of the entire data set [10]. The empirical K-function for a data set is calculated as

$$\hat{K}(r) = \frac{|W|}{n(n-1)} \sum_{i=1}^{n} \sum_{\substack{j=1 \\ j \neq i}}^{n} \mathbf{1}\{d_{ij} < r\} e_{ij}(r), \tag{1}$$

Where $|W|$ is the volume of a data set, n is the number of data points, d_{ij} is the distance between points i and j, $\mathbf{1}$ is the indicator function (i.e. $\mathbf{1} = 1$ if $d_{ij} < r$, $\mathbf{1} = 0$ if $d_{ij} \geq r$), and $e_{ij}(r)$ is an edge correction weight to correct for points on the edge of the data set. [11]

The "expected" output of this function corresponds to a random point distribution. If there are more points than expected within a certain radius, then the data is clustered. If there are fewer points than expected, then the data is inhibited, or regular [10]. The K-function gives information about relationships over the entire data set.

The main use of the K-function is to test the hypothesis of complete spatial randomness (CSR) in a spatial data set. To do this, it is necessary to first construct random relabeling (RRL) envelopes from the data. This is done by taking the full point cloud, randomly selecting some set percentage of points, and measuring the empirical K function on this subset of known CSR points. This process is repeated many thousands of times to create acceptance interval (AI) envelopes for the K-function [11]. These envelopes give upper and lower bounds for where we might observe a K-function if the data we are observing is truly random. These envelopes can be built at any probability. For example, constructing the 99% AI envelope means that 99% of the random samples' K-function fall inside of the envelope. Then, if the observed K-function of a real data set falls outside of this envelope, there is only a 1% chance that it came from a CSR data set, so we conclude that the data set is not CSR. If the observed K-function falls above the envelope, we can say that there is statistically significant evidence of clustering, while if it falls below the envelope, there is significant evidence of inhibition.

Transformations on the empirical K-function make it easier to visually interpret. In this paper, we use a transformed version of the empirical $\hat{K}(r)$ function, which we call $\sqrt{\hat{K}(r)}$ anomaly. This function is defined as

$$\sqrt{\hat{K}(r)} \text{ anomaly} = \sqrt{\hat{K}(r)} - \text{median of RRL}.$$

In other words, we take the square root of the original K-function and then subtract off the median of the random relabelings at each r value. The square root normalizes variance across the r values [11], while subtracting off the median of the RRLs centers the random envelopes around zero, so that they are easier to interpret on plots.

Figure 1 shows an example of a measured $\sqrt{\hat{K}(r)}$ anomaly from a clustered data set, along with the associated RRL acceptance interval envelopes. It is clear that there is statistically significant evidence of clustering on $1 < r < 5$ and significant inhibition on $6 < r < 8$. While the main purpose of the K-function in literature has been a binary conclusion of clustered vs not-clustered, there is likely more information about the spatial data set contained in the results of the K-function. A main objective of this paper is trying to extract this information about clustering from the output of the K-function.

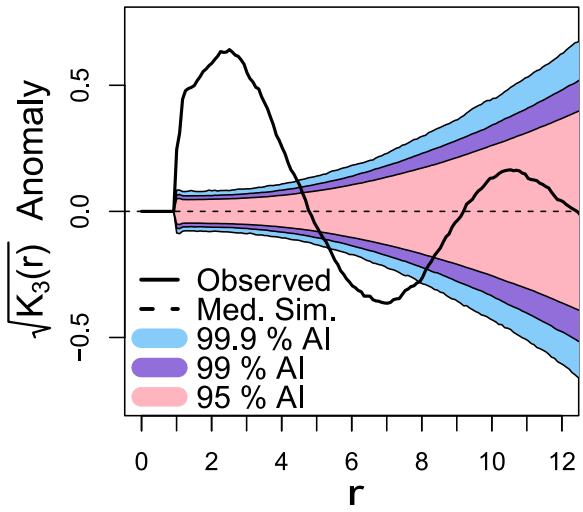

Figure 1: Example of $\sqrt{\hat{K}(r)}$ anomaly measured on a clustered data set (black line), shown on top of RRL acceptance interval envelopes.

There are other functions similar to the K-function that are used to analyze relationships in spatial data, although they are not explored very heavily in this paper. One is the G-function, or nearest neighbor distribution, which calculates the cumulative distribution function (CDF) for first nearest neighbor distance between points. The empirical G-function for a data set is calculated as

$$\hat{G}(r) = \frac{1}{n} \sum_{i=1}^{n} \mathbf{1}\{d_i \leq r\}, \tag{2}$$

where d_i is the nearest neighbor distance for point i [11]. Another similar function is the F-function, or empty space function, which calculates the CDF for distance to the nearest point from a regularly spaced grid. The empirical value is calculated as

$$\hat{F}(r) = \frac{1}{m} \sum_{j=1}^{m} \mathbf{1}\{d_j \leq r\}, \tag{3}$$

where there are m points in the regularly spaced grid, and d_j is the distance from point j of this grid to its nearest neighbor in the data set [11]. The G and F functions and give information about local point relationships.

When dealing with point patterns containing two types of points, as is the case with OLED data, the K and G-functions can be applied either to one type of points, or across the two types. When applied to only one type, the functions return information about how points of the same type are spatially related to one other. When applied across point types, the K-function calculates the average number of points of type A that lie within any point of type B, or vice versa. The G-function calculates the PDF of first nearest neighbor distances from points of type A to points of type B or vice versa [11]. The equations for these functions are similar to those presented for the homogeneous cases above. These "cross" functions return information about how points of different types are spatially related to one another. While all of these spatial functions have the potential to be used to analyze APT data to find aggregation within the emissive layer of OLED molecules, we mostly focus on the K-function in this paper. There is more exploration to be done on what the G and F functions can tell us about our data.

If the spatial statistics tell us that there is general clustering behavior in a sample, there are many computer algorithms designed to detect and isolate which points in the data set lie within clusters [4]. It is unclear whether these algorithms will be able to isolate definite clusters from the often weak clustering behavior of emitter molecules in OLEDs, but they have been shown to work in other APT data with distinct clustering behavior [5, 6]. If applicable, these algorithms will allow for the further study of individual cluster properties such as density, shape, and spacing.

2.4 Our New OLED Cluster Research

Emitter molecule clustering in OLEDs can be better quantified using APT and spatial statistics. In this paper, we detail our methodology and results in connecting the functions described above to specific cluster properties like cluster size, shape, and density. This will eventually lead to a better understanding of structure-performance relationships in OLEDs, which can then be used to design more efficient and longer lasting light sources.

3 Methods

We first used simulations of OLED structure to study what the results from the spatial statistics functions described in Section 2.3 reveal about the structure of an OLED emissive layer from its APT data. Simulations for the emissive layer of OLEDs were driven by its known properties; It has an amorphous structure and the molecules do not overlap [1]. One model that fits both of these requirements is random close packed (RCP) spheres. RCP is defined as a random packing of objects with packing fraction so large that any increase would force the objects into an ordered (crystal) structure [12]. For our simulations, we generate a set of RCP spheres using a computer algorithm [13] and take the center of the spheres as molecule positions, like they would be returned from APT. This imitates the random behavior and inhibition of the small organic molecules well.

Once this background molecular structure has been generated, we turn it into an emissive layer by labeling a certain percent of the points as emitter molecules, and labeling the rest as host molecules. The emitter molecules can be placed in different controlled clustered configurations. Specifically, we simulate spherical clusters with normally distributed radii, spaced in an expanded RCP pattern. We have control over mean cluster radius, radius standard deviation, inner-cluster density of points, overall density of points, and amount of Gaussian blur of cluster center positions off of the original RCP grid. The advantage to simulating this spatial data is that we have complete control and knowledge over the structure of the emitter molecule clusters, which means that we know what properties we are trying to gather from our analysis methods before we apply them. This allows us to study the accuracy and uncertainty of these methods.

We first used these simulations to study the K-function. To do this, we tracked different metrics from the output of the empirical K-function applied to clustered data as we changed different clustering properties. The metrics that we collected are different positions and amplitudes of the K-function and its derivatives. An example of the five specific metrics we collect is shown in Figure 2. Our goal was to determine a relationship between these metrics and specific cluster properties. To do this, we tracked these metrics while measuring the K-function on clustered data sets with different combinations of the properties that we have control over. Each combination of cluster properties was simulated 101 times so that we could measure the variance of the K-function between data sets with the same properties.

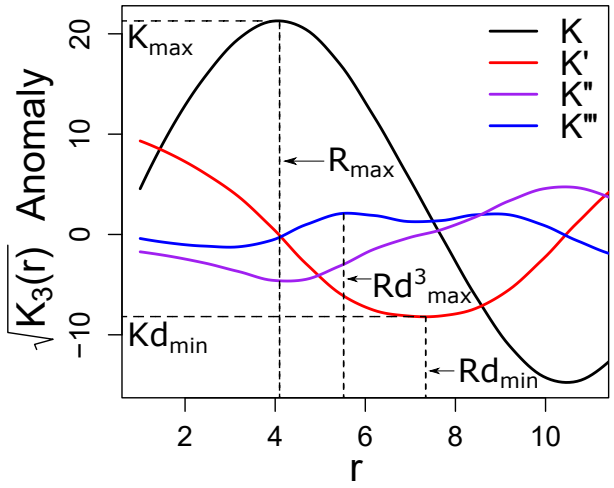

Figure 2: Example K-function showing the 5 metrics which we extracted from the results of each spatial data set. The black line is the measured K-function while the colored lines are higher order numeric derivatives of this result.

Using the Mines high-performance computing (HPC) system, we were able to simulate 15,000 sets of clustered spatial data, each with a different combination of the cluster properties we have control over. We then measured the empirical K-function on each of these data sets, and extracted the metrics showed in Figure 2. Once we had this large data set, we trained machine learning models to predict cluster properties from the K-function metrics. We used machine learning models instead of a more interpretable model because after some

exploration, we discovered that the relationships between metrics and properties were quite complex, non-linear, and correlated. This made machine learning the most viable way to extract these relationships into a model.

Once these machine learning models are fully developed, we will be able to apply the K-function to real APT data and make conclusions about cluster properties and the uncertainty of our conclusions based on the simulation work. We wrote all of the code for this analysis in R and C, so the properties and uncertainties of APT data can be extracted automatically without too much extra work.

Another important property of the K-function which we are interested in exploring is how the volume of the spatial data set to be analyzed impacts the variance of the results. APT machine time can be expensive, and the larger the material sample, the longer it takes to complete, so minimizing sample size as much as possible is important to minimize the cost to our group.

There is always some inherent variation in the results from the K-function, even when performed on two sets of data that contain the exact same properties (this is why we need to do RRL to develop envelopes to test for randomness). As the volume of the sample goes up, there is more data to average the K-function out, so the variation reduces. For our materials, our radii of interest are in the 5-10 nm range, so we want the sample volume to be large enough so that the variation of the K-function at these radius values is low. We studied this impact by looking at the RRL envelopes and clustering envelopes of the same data windowed at different volumes. Clustering envelopes are similar to RRL envelopes; we simulate multiple realizations of clusters with the exact same properties, but different random seeds, to get an idea of how the K-function varies when performed on clustered data sets with the exact same properties.

The last analysis of the K-function that we performed was modeling it's output based on cluster properties as inputs. The goal was to come up with a completely symbolic model for the K-function output as a function of cluster properties. We could then relate cluster properties directly to K-function metrics and have derived theoretical predictions for what each metric should tell us about the spatial data.

Moving forward, we plan on doing a similar analysis as we did on the K-function with the G and F-functions. We have not yet determined which metrics we are going to track from these functions, but we anticipate that adding some of these metrics as inputs to our machine learning models will increase their accuracy.

The results from this analysis will be the first ever quantification of emitter molecule clustering within OLEDs, and will open the door for others in our group to perform experiments aimed towards a better understanding and quantification of the connection between material structure and performance.

4 Results

First, we will discuss the results of the cluster property models based on K-function metrics. One challenge we ran into while training these models was in predicting mean cluster size when there was a large distribution of cluster sizes through the data set. This challenge is due to the fact that when there is a distribution of cluster sizes, the K-function weights

itself more towards the larger clusters than the smaller clusters because larger clusters have more points in them. This means that the K-function has difficulty distinguishing between a uniform cluster size pattern with larger clusters, and a distributed cluster size pattern with lower mean but higher standard deviation. To deal with this problem, we came up with a new property called the weighted radius. It is defined as

$$r_w = \frac{\mathbb{E}[r \times \frac{4}{3}\pi r^3]}{\mathbb{E}[\frac{4}{3}\pi r^3]}.$$

It is essentially the average cluster radius, weighted by the volume that each radius creates. This means that the weighed radius is also weighted towards larger clusters, and is therefore suited for the K-function to measure. The weighted radius is a function of both the mean and variance of the distribution of cluster size in a data set. For a normal distribution with mean μ and variance σ^2, which is what we used to simulate clusters in this paper, the equation for weighted radius is

$$r_w = \frac{\mu^4 + 6\mu^2\sigma^2 + 3\sigma^4}{\mu^3 + 3\mu\sigma^2}.$$

We trained a variety of machine learning models for weighted radius and cluster density based on the 15,000 clustered data set simulations, and found that a random forest (RF) regression worked best for predicting properties from K-function metrics. We trained these models using 75% of the simulations and tested them on the remaining 25%. While RF regression was the model that had the lowest error in each case, we tested a variety of models. Table 1 shows the RMSE values for each tested model on the test data set. From this table, it is evident that the RF models did the best job minimizing error for both models, so these are the models we chose to use moving forward.

Table 1: RMSE of Machine Learning Models on Test Data

Model Name	Weighted Radius Model RMSE	Cluster Density Model RMSE
Baysian Regulated Neural Network	0.132	0.0135
Generalized Linear Model	0.269	0.0430
Elastic-Net Linear Model	0.269	0.0430
K Nearest-Neighbors	0.254	0.0183
Random Forest	0.118	0.0123

We are happy with the RF weighted radius model's root mean square error (RMSE) of 0.1181 and the RF cluster density model's RMSE of 0.0123. Note that cluster density ranges

from 0 to 1, and represents the percentage of background points in the cluster which are marked as emitter molecules. The proper word for this is probably "concentration", but we took to calling it density through the year, so I stuck with that usage in this paper. The results of the RF model's predictions of the test data for both weighted radius and cluster density are shown in Figure 3.

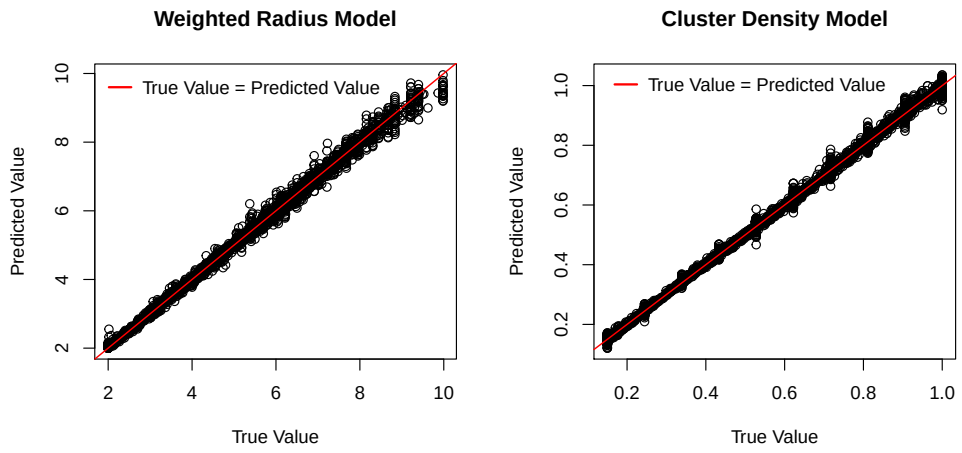

(a) Weighted radius model (b) Inner-cluster density model

Figure 3: Random forest models that achieved lowest RMSE for the two properties that we are happy with.

So, out of the four properties that we had control over in our simulation (mean cluster radius, standard deviation of cluster radius, cluster density, and cluster separation), we have a model to extract cluster density directly, and to extract mean and standard deviation of cluster radius indirectly through the weighted radius. One problem with the weighted radius is that we have no way to un-couple mean and standard deviation. We need to develop some other metric which can distinguish between the two. This is something we hope to work on in the future.

With these models, we now have the ability to measure weighted radius and cluster density in APT data where we do not know what the real properties are. We have made some large assumptions about the type of clustering that may be occurring in the OLED materials; perfectly spherical clusters are unlikely. However, using these models will give us a reasonable estimate of the clustering occurring in our APT data.

Next, we will look at the analysis of sample volume's impact on the variability of the K-function. We looked at RRL and cluster envelopes from the same spatial data sets, but windowed down to different volumes. Specifically, we looked at cubic volumes of 20x20x20 nm, 40x40x40 nm, and 60x60x60 nm, and non-cubic volumes of 20x60x60 nm and 40x60x60 nm. For each volume, we calculated the 99% acceptance interval envelopes for random relabeling, and the 95% acceptance interval for cluster envelopes. As mentioned in section 3, our goal is to get low variation in these envelopes at radius values from 5-10 nm. Figure 4 shows both the RRL envelopes and the cluster envelopes for each volume analyzed.

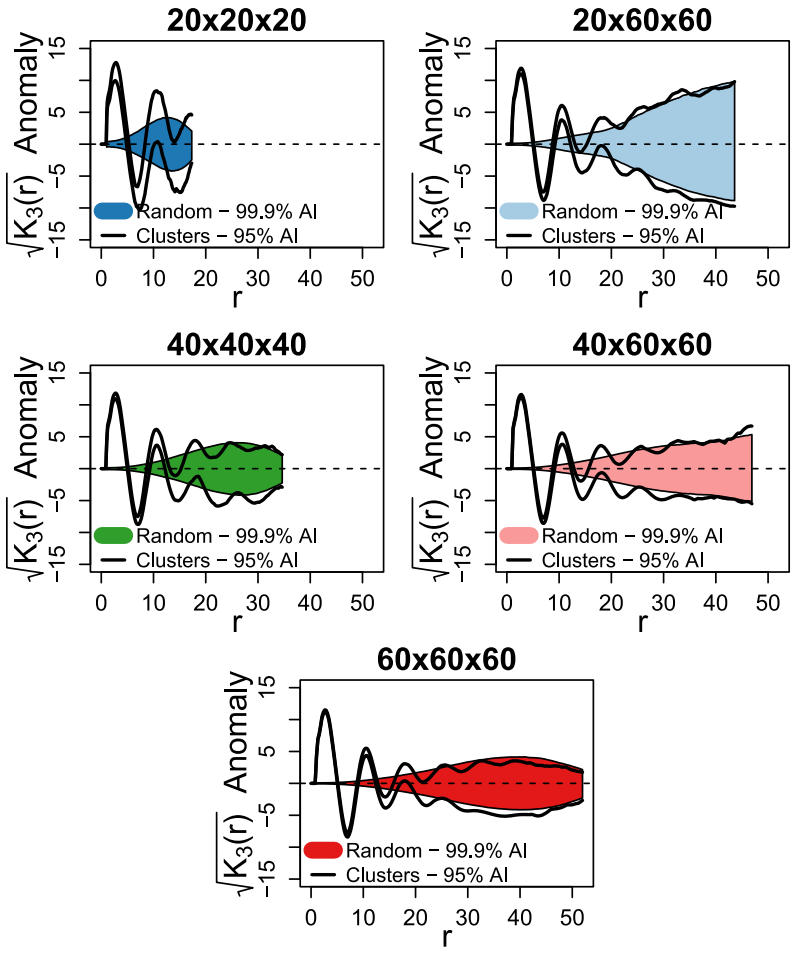

Figure 4: Random relabeling envelopes and cluster envelopes for $r = 3$ spherical clusters with 100% density, no background density, and RCP spacing. Each plot is for a different volume size.

It is evident from Figure 4 that once we get up to the 60x60x60 nm volume, both the RRL and the cluster envelopes are very small, indicating small variation in the K-function for both random and clustered data. Because of this, we decided that we need to get at least a 60x60x60 nm cube's worth of data from APT measurements of our materials. This is an important conclusion, as the group was previously using 20x40x40 nm volumes to analyze data. Using this analysis, it is evident that this volume is not large enough for the K-function to be consistent at our radius values of interest.

Lastly, we will discuss our model for the K-function. The original plan was to come up with a model that was purely symbolic and a function of cluster properties. Unfortunately, the K-function turned out to be much more complicated than we originally anticipated. We still came up with a model, but it needs to be evaluated numerically in Mathematica at each radius value, so it cannot be used to symbolically relate cluster properties to the K-function. Our model accurately predicts the empirical K-function output for uniformly sized well spaced clusters with a specific cluster density, background density, and overall density. As far as we know, this is the first model for the K-function of clustered data that includes

the background noise. Background noise, or points which are in the pattern but not in any clusters, create some strange behavior with K-function output, so it is important to include it in any attempt to model K-function behavior. The model is

$$K_3(r) = \frac{1}{\sigma_1 V_1 + \sigma_2 V_2}\left[\frac{\sigma_1 V_1 \int_{V_1}(\sigma_1 V_i(r,r') + \sigma_2 V_o(r,r'))d^3r'}{\sigma_3 V_1} + \frac{\sigma_2 V_2 \int_{V_2}(\sigma_1 V_i(r,r') + \sigma_2 V_o(r,r'))d^3r'}{\sigma_3 V_2}\right], \quad (4)$$

where each parameter in equation (4) is described in Table 2.

Table 2: Parameter Definitions for Equation (4)

Variable	Meaning
σ_1	Inner-cluster density
σ_2	Background density
σ_3	Overall density
V_1	Volume of spherical cluster ($\frac{4}{3}\pi R^3$)
V_2	Volume of background within space filling polyhedron
$V_i(r,r')$	Volume of sphere with radius r centered at r' that intersects any surrounding cluster
$V_o(r,r')$	Volume of sphere with radius r centered at r' that does not intersect any surrounding cluster

Figure 5 shows an example of how this model fits an actual measured K function. The model predictions in this figure are the blue dots, and are interpolated with the blue dotted line, while the measured K-function from a simulated data set is shown as the red line. For this plot, clusters were simulated with radius = 3, inner-cluster density (as a percentage of points in the spheres) = 50%, background density = 3%, overall density of 7.5%, and cluster spacing of 12 nm. This was just a random selection of parameters which shows the ability of the model to accurately predict the K-function in a data set with background density.

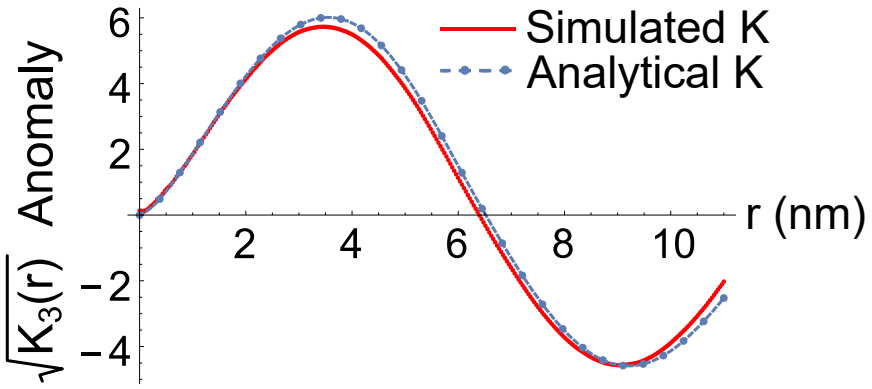

Figure 5: Model K-function from equation (4) shown over a measured K-function with same cluster parameters.

It is clear from Figure 5 that the model does an excellent job predicting output from the K-function. There is some slight variation between the two lines, which we believe is due to some approximations that Mathematica performs while doing numeric integration to evaluate the model.

5 Conclusions

We were able to successfully find methods to measure cluster size (weighted radius), and inner-cluster density in 3D spatial point patterns using Ripley's K-function. These methods can be applied to real material data from APT in order to quantify and characterize the clustering of emitter molecules in a given material sample. We were also able to determine what sample volume is required to obtain consistent results from the K-function. This volume will drive the size of material samples that our research group measures with APT. Lastly, we found a model of the empirical K-function for clustered spatial data, even in the presence of background points.

These results will be used to help determine which OLED fabrication conditions minimize clustering of the emitter molecules, with the end goal of increasing OLED efficiency and lifetime to make them more viable as a cheaper alternative to synthetic LEDs common in the electronics industry today.

6 Future Work

I will continue to do research on this subject next year while I pursue a master's degree in statistics here at Mines. During this time, we hope to explore other spatial statistics functions like the G and F-functions described in section 2.3 to extract different information from APT data. Specifically, we want to be able to break the weighted radius down into its components of mean radius and standard deviation of radius.

Additionally, we are just now beginning the process of analyzing APT data from OLEDs. The APT machine has been broken for this whole year, so we have had issues getting data

to apply these cluster quantification methods to. However, graduate students in our group have recently been able to gather data using the APT machine at NIST in Boulder, so we have some brand new data that we will begin applying these methods to very soon.

Lastly, we plan on eventually looking into the cluster detection algorithms described in section 2.3 so we can analyze more specific cluster properties of material samples than spatial statistics can give us.

7 Cost Analysis

As this project is based in simulation work using the free programming languages R and C, it has required no physical consumables or software costs. As a result of this, the only costs for this project were labor and overhead. I worked 8 hours per week for 15 weeks each of first and second semester this year. This adds up to 240 hours of work at a hourly wage of $11.00, or $2,640.00 of total labor cost. Overhead was approximately 50% of this value, which is $1,320.00. This sums to a total project cost of $3,960.000. This cost analysis is summarized in Table 3.

Table 3: Project cost analysis

Item	Unit Cost	Quantity	Unit	Cost ($)
Labor - 1 student	$11.00	240	hr	2,640.00
Overhead - 50% of labor	–	–	–	1,320.00
			Total cost	$3,960.00

References

[1] N Thejo Kalyani and SJ Dhoble. Organic light emitting diodes: Energy saving lighting technologya review. *Renewable and Sustainable Energy Reviews*, 16(5):2696–2723, 2012.

[2] W Staroske, M Pfeiffer, K Leo, and M Hoffmann. Single-step triplet-triplet annihilation: An intrinsic limit for the high brightness efficiency of phosphorescent organic light emitting diodes. *Physical review letters*, 98(19):197402, 2007.

[3] David N Seidman and Krystyna Stiller. An atom-probe tomography primer. *MRS Bulletin*, 34(10):717–724, 2009.

[4] Rui Xu and Donald Wunsch. Survey of clustering algorithms. *IEEE Transactions on neural networks*, 16(3):645–678, 2005.

[5] W Lefebvre, T Philippe, and F Vurpillot. Application of delaunay tessellation for the characterization of solute-rich clusters in atom probe tomography. *Ultramicroscopy*, 111(3):200–206, 2011.

[6] Leigh T Stephenson, Michael P Moody, Peter V Liddicoat, and Simon P Ringer. New techniques for the analysis of fine-scaled clustering phenomena within atom probe tomography (apt) data. *Microscopy and Microanalysis*, 13(6):448–463, 2007.

[7] H van Eersel. *Device physics of organic light-emitting diodes: interplay between charges and excitons*. PhD thesis, Technische Universiteit Eindhoven, 2015.

[8] Sebastian Scholz, Denis Kondakov, Bjorn Lussem, and Karl Leo. Degradation mechanisms and reactions in organic light-emitting devices. *Chemical reviews*, 115(16):8449–8503, 2015.

[9] Andrew P Proudian, Matthew B Jaskot, David R Diercks, Brian P Gorman, and Jeramy D Zimmerman. Atom probe tomography of organic molecular materials: Subdalton nanometer-scale quantification. *arXiv preprint arXiv:1806.10650*, 2018.

[10] Philip M Dixon. Ripley's k function. *Wiley StatsRef: Statistics Reference Online*, 2014.

[11] Baddeley Adrian, Rubak Ege, and Turner Rolf. Spatial point patterns: Methodology and applications with r, 2015.

[12] R Frost, JC Schön, and P Salamon. Simulation of random close packed discs and spheres. *Computational materials science*, 1(4):343–350, 1993.

[13] Kenneth W Desmond and Eric R Weeks. Random close packing of disks and spheres in confined geometries. *Physical Review E*, 80(5):051305, 2009.